MODELLING PROCESS-INDUCED DEFORMATIONS IN COMPOSITE STRUCTURES USING HIGHER ORDER ELEMENTS

Abdul Rahim A Arafath, Reza Vaziri and Anoush Poursartip
Departments of Civil Engineering & Materials Engineering
The University of British Columbia
Vancouver, BC, Canada

Keywords: ***Composites, Processing, Residual stresses, Warpage, Higher-order finite element***

Abstract

During the processing of thermoset-based composite structures, the thermal strain mismatch between the part and the tool induces a steep stress gradient through the thickness of the part. Capturing this stress gradient which occurs at the initial stages of the curing process is the key for successful prediction of process-induced deformations using the finite element method. The number of elements necessary for accurate through-thickness resolution varies from problem to problem. Successive mesh refinement to achieve convergence is a tedious and costly proposition. To address this issue, two higher-order finite elements based on h- and p-adaptive techniques are developed in this study to enable accurate solutions to various processing problems using a single element discretization through the thickness. Examples are presented to demonstrate the efficacy of these elements.

1 Introduction

As the resin cures during the processing of thermoset-based composite structures, its effective elastic (and shear) modulus increases by as much as 6 orders of magnitude from roughly 1 kPa to 1 GPa. In the heat-up phase the tool expands and stretches the part with it thus inducing a steep gradient of stress through the thickness due to the low shear modulus of the part. This stress gradient locks in as the material cures which upon removal of the tool, causes the part to warp. It is crucial to capture the stress gradient that occurs at the initial stages of cure in order to predict the residual deformation of the composite part accurately [1]. Using mechanistic closed-form solutions [2], the authors have shown that the through-thickness stress gradient depends on both material and geometrical properties of the part.

Solid elements are commonly employed to model process induced deformations since classical shell elements are not able to capture such highly nonlinear through-thickness stress gradients accurately. However, the main drawback of using solid elements is that a rather large number of such elements are often necessary for spatial discretization in order to satisfy accuracy requirements while avoiding the locking effect that occurs in solid elements with large aspect ratios. In recent years, many shell-like solid element formulations have been reported in the literature, with the intent of eliminating the locking effects. Recently, Dhondt [3] showed that 20-noded solid elements with reduced integration are effective in modelling thin-walled (shell-like) structures. Even though this will allow us to use a large aspect ratio, one still needs more than one element (up to 8 elements) in the thickness direction to capture the large stress gradients that occur during the initial stages of cure. Since the stress gradient depends on the material and geometrical properties [2], the number of elements in the thickness direction varies from problem to problem. Finding the number of elements necessary in the thickness direction for a particular problem by trial-and-error is ineffective and costly.

Adaptive mesh refinement has been the subject of extensive investigation with the objective of obtaining solutions with pre-specified accuracy with minimum cost of model preparation and computation [4,5]. The two main categories of refinements are the *h*-refinement and the *p*-refinement. In adaptive *h*-refinement, a mesh with a fixed type of low order elements is successively refined by reducing the size of the elements. By

contrast, in adaptive *p*-refinement the elements of the mesh remain fixed in both size and position while the polynomial order, *p*, of the shape functions is enriched by adding higher order terms to the existing lower order shape functions.

In this study, the above two adaptive methods are used to render the process modelling more efficient by (i) eliminating the need for explicit meshing through the thickness, and (ii) selecting the number of degrees of freedom (d.o.f) automatically during the computational run on an as-needed basis.

2 Element Formulation

In this section two types of higher order elements are described based on using the *h*- and *p*-refinement techniques through the thickness direction only. The basic element has 24-nodes in total (8 on each of the bottom, top and mid planes) as shown in Fig. 1.

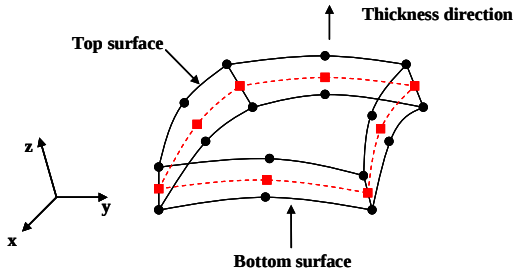

Fig. 1. 24-node hierarchical solid element

The bottom and top surface nodes have the 3 conventional displacement d.o.f's (*u*, *v* and *w*). The number of d.o.f's at the mid-plane nodes varies depending on the number of terms used in the *p*-refinement or the number of element-layers used implicitly in the *h*-refinement techniques. In the *p*-refinement, the d.o.f's at the mid-plane nodes are merely unknowns that do not have any physical meaning. However, in the *h*-refinement, the d.o.f's at the mid-plane nodes correspond to the displacements in the various element layers through the thickness.

The developed element is a composite element with multiple numbers of layers. The layers may be of the same material with different fibre orientations or different materials (e.g. hybrid or sandwich panels) and are assumed to be stacked in the thickness direction. The layer thicknesses can vary arbitrarily within the element. The layer thickness at an integration point can be found by linear interpolation of layer thicknesses defined at the four corner nodes [6]. Both the *h*- and *p*-elements have been developed and implemented in ABAQUS [7] as user defined elements. The evolving properties of the composite material during the curing process are modelled using the COMPRO Component Architecture (CCA) approach [8].

2.1 Numerical Integration

The element stiffness matrix in the local element coordinate is given by:

$$\boldsymbol{K} = \int_{-1}^{1}\int_{-1}^{1}\int_{-1}^{1} \boldsymbol{B}^T \boldsymbol{D}\, \boldsymbol{B} \left|\boldsymbol{J}\right| d\xi\, d\eta\, d\zeta \qquad (1)$$

where $\left|\boldsymbol{J}\right|$ is the determinant of the Jacobian matrix, $\boldsymbol{B}$ and $\boldsymbol{D}$ are the strain-displacement (small strains) and material stiffness matrices, and ξ,η,ζ are the element natural co-ordinates.

The above integral is evaluated numerically using the combination of Gaussian quadrature and Simpson's rule (Fig. 2).

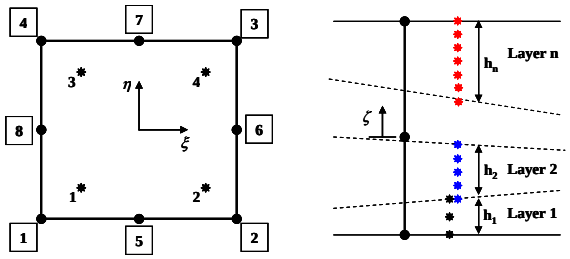

Fig. 2. Schematic showing the in-plane and through thickness integration points in the 24-noded composite solid element

A 4-point reduced Gauss integration is used in-plane to avoid the locking effects. The reduced integration is necessary only in the in-plane direction [9] while full integration is used in the through-thickness direction to capture the details of the stress distribution.

The material stiffness matrix $\boldsymbol{D}$ varies from layer to layer and thus is not a continuous function of ζ. Therefore the integration is carried out layerwise in order to obtain the stiffness coefficients for the entire element. For the layerwise through-thickness integration both the Gauss and Simpson's rules are used.

In order to apply the usual weight factors in the Gaussian and Simpson's formula, the co-ordinate limits for the layer thickness have to be -1 and +1. This can be achieved by suitably modifying the variable ζ to ζ_k in layer k such that ζ_k varies from -1 to +1 in that layer:

$$\zeta = -1 + \frac{1}{t}\left[-t_k \left(1 - \zeta_k\right) + 2\sum_{j=1}^{k} t_j \right] \qquad (2)$$

where t is the total thickness and t_k is the k^{th} layer thickness. Now the integral in Eq. (1) becomes:

$$\boldsymbol{K} = \sum_{k=1}^{n} \int_{-1}^{1}\int_{-1}^{1}\int_{-1}^{1} \boldsymbol{B}^T \boldsymbol{D_k}\, \boldsymbol{B} \left|\boldsymbol{J}\right| \frac{t_k}{t} d\xi\, d\eta\, d\zeta_k \qquad (3)$$

Generally, in a composite element, at least one Gauss point per layer is required to capture the effect of different layer properties. If Simpson's integration scheme is adopted, at least three integration points per layer are needed in the thickness direction. In a typical composite laminate involving multiple layers the number of integration points per layer should be sufficient to integrate the higher order terms accurately. The efficiency of the run time is very sensitive to the number of integration points used to calculate the load vectors and stiffness matrices. Even though our goal is to achieve overall efficiency in process modelling, the main focus here is on automating the process of selecting the number of elements in the thickness direction, so that the pre-processing time can be reduced or the costly successive mesh refinment technique for obtaining a converged solution can be eliminated.

2.2 Displacement Interpolation Functions

The in-plane interpolation (shape) functions are similar to the shape functions of a 2-dimensional conventional serendipity 8-noded solid element. The eight in-plane shape functions (Q_n) are given by:

$$\begin{aligned}
Q_i &= \frac{1}{4}(1+\xi\xi_i)(1+\eta\eta_i)(\xi\xi_i + \eta\eta_i - 1)\\
Q_5 &= \frac{1}{2}(1-\xi^2)(1-\eta)\\
Q_6 &= \frac{1}{2}(1+\xi)(1-\eta^2)\\
Q_7 &= \frac{1}{2}(1-\xi^2)(1+\eta)\\
Q_8 &= \frac{1}{2}(1-\xi)(1-\eta^2)\\
&\text{where} \quad i = 1 \cdots 4
\end{aligned} \qquad (4)$$

The shape function corresponding to each surface nodes are obtained by multiplying the in-plane shape functions with the corresponding through-thickness shape functions. If the through thickness shape function corresponding to the bottom, top and mid surface are given by R_b, R_t and R_m respectively, then the nodal shape functions can be written as:

$$\begin{aligned}
N_i &= Q_i R_b && \text{Bottom surface nodes}\\
N_{i+8} &= Q_i R_t && \text{Top surface nodes}\\
N_{i+16} &= Q_i R_m && \text{Mid surface nodes}\\
&\text{where} \quad i = 1 \cdots 8
\end{aligned} \qquad (5)$$

The displacement interpolation is given by:

$$\mathrm{u} = \sum_{i=1}^{nu} N_i\, u_i,\ \mathrm{v} = \sum_{i=1}^{nv} N_i\, v_i,\ \mathrm{w} = \sum_{i=1}^{nw} N_i\, w_i \qquad (6)$$

The number and form of the shape functions N_i depend on the type of elements used (*h*- or *p*-refinement). The details of the shape functions will be presented below.

2.2.1 Hierarchical Element

In the hierarchical element formulation, the order of the through-thickness displacement interpolation is increased by adding extra d.o.f's to the mid-surface nodes. The basic element has a quadratic interpolation function with 3 d.o.f's at each of the mid-plane nodes. The displacement fields are discretized as follows:

$$\begin{aligned}
u &= \sum_{i=1}^{16} N_i\, u_i + \sum_{i=17}^{24} N_i\, a_i\\
v &= \sum_{i=1}^{16} N_i\, v_i + \sum_{i=17}^{24} N_i\, b_i\\
w &= \sum_{i=1}^{16} N_i\, w_i + \sum_{i=17}^{24} N_i\, c_i
\end{aligned} \qquad (7)$$

Only the order of interpolation for u and v are increased and the through-thickness interpolation function for w remains quadratic. The order of the interpolation function can be increased by one order through the introduction of two more d.o.f's at the mid-surface nodes (total of 16 d.o.f's).

$$\begin{aligned}
u &= \sum_{i=1}^{16} N_i\, u_i + \sum_{i=17}^{24} N_i\, a_i + \sum_{i=25}^{nu} N_i\, a_i\\
v &= \sum_{i=1}^{16} N_i\, v_i + \sum_{i=17}^{24} N_i\, b_i + \sum_{i=25}^{nv} N_i b_i\\
w &= \sum_{i=1}^{16} N_i\, w_i + \sum_{i=17}^{24} N_i\, c_i
\end{aligned} \qquad (8)$$

The shape function for a 3rd order hierarchical element is shown in Fig. 3.

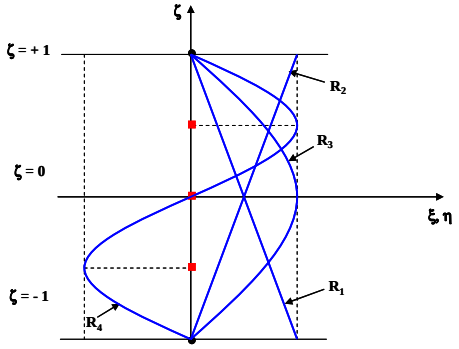

Fig. 3. Through-thickness displacement interpolation functions for a 3rd order hierarchical element

Many different types of shape functions can be used for the hierarchical shape functions [4-5]. The only requirement is that they have zero values at the top and bottom nodes. Due to their orthogonal properties, the most commonly used shape functions for hierarchical elements are the Legendre polynomials [4-5]. In this study, Legendre polynomials are used thus resulting in the following through-thickness shape functions:

$$R_1 = \frac{1}{2}(1-\zeta)$$
$$R_2 = \frac{1}{2}(1+\zeta) \qquad (9)$$
$$R_3 = \phi_{i-1} \qquad i = 3,4,\ldots(p+1)$$

where ϕ_i is given by:

$$\phi_j = \frac{1}{\sqrt{4j-2}}\left(P_j - P_{j-2}\right)$$
$$P_k = \frac{1}{2^k k!}\frac{d^k}{d\xi^k}\left(\xi^2-1\right)^k \qquad (10)$$
$$\text{where} \quad j = 2,3,\ldots \text{and} \quad k = 0,1,2\ldots$$

where P_k are the Legendre polynomials and p is the polynomial order by which the element is identified.

2.4.2 Layer-wise Element

In the layer-wise element method, each layer is a quadratic 24-noded element. The through-thickness shape function for such an element is quadratic and for a one-layer element can be written as:

$$R_1 = \frac{1}{2}\left(\zeta^2 - \zeta\right)$$
$$R_2 = \frac{1}{2}\left(\zeta^2 + \zeta\right) \qquad (11)$$
$$R_3 = \left(1-\zeta^2\right)$$

An additional element-layer can be added to the element by introducing two more nodes in the thickness direction as shown in Fig. 4(b). To add physical nodes, a new mesh needs to be generated. However, to avoid mesh regeneration an element-layer can be added through the introduction of additional d.o.f's at the mid-nodes.

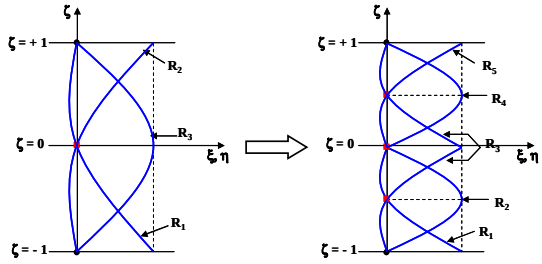

(a) (b)

Fig. 4. Through-thickness displacement interpolation functions for layer-wise elements: (a) one-layer and (b) two-layer elements

The main restriction of the current layer-wise approach is that the number of element layers cannot be dynamically added or dropped during the computational analysis. The number of element layers necessary for a problem is selected a prior and then kept constant throughout the analysis. However, the process of selecting the necessary number of element layers can be automated based on the material and geometrical parameters of the domain being discretized.

3 Verification Examples

3.1 Varying Layer Thickness

A benchmark example is used here to test the capability of the developed element to model varying layer thicknesses in a composite element. A cantilever tapered sandwich beam, as shown in Fig. 5, is analysed for this purpose.

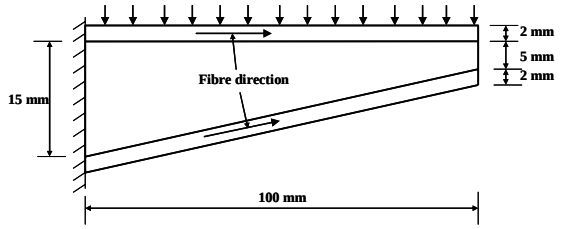

Fig. 5. Schematic of a tapered sandwich beam with a varying thickness core under a uniformly distributed load

The sandwich beam is assumed to consist of a tapered aluminum core with unidirectional CFRP composite skins. In practice, a softer material than aluminum is commonly employed for the core. However, this would require more than one element discretization in the thickness direction in order to capture the highly non-linear through-thickness distribution of the in-plane displacements resulting from the transverse shear compliance of the beam. With the aluminum core, one element through the thickness is sufficient to model the beam. The properties of the skin and core materials are listed in Table 1.

Table 1. Properties of the CFRP skin and aluminum core

Properties	CFRP Skin	Aluminum Core
E_{11} (GPa)	126	69.0
$E_{22} = E_{33}$ (GPa)	10.2	69.0
$\nu_{12} = \nu_{12}$	0.265	0.327
ν_{23}	0.467	0.327
$G_{12} = G_{13}$ (GPa)	5.44	26.0
G_{23} (GPa)	3.46	26.0
CTE_1 (μ/°C)	0.0374	23.6
$CTE_2 = CTE_3$ (μ/°C)	29.5	23.6

The beam is subjected to a uniformly distributed load on the top surface. Both the ABAQUS built-in 20-noded element and the current 24-noded element are used to model the beam. For the 20-noded element, each of the skins and the core are modelled with single elements in the thickness direction, since the ABAQUS composite elements do not accommodate varying layer thicknesses. In the 24-noded element case, the whole thickness of the beam is modelled with just one element. A comparison of the predicted deflection profiles using these elements are shown in Fig. 6. It can be seen that the two predictions agree quite well thereby instilling confidence in the implementation of the varying layer feature of the developed user defined element in ABAQUS.

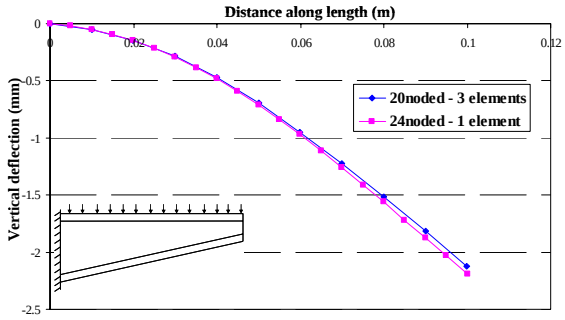

Fig. 6. Comparison of the predicted deflection profiles of a tapered sandwich beam using the ABAQUS built-in 20-noded element and the developed 24-noded user element

3.2 Performance of *h*- and *p*-Elements

In this section we compare the convergence rates and efficiencies of the developed *h*- and *p*-elements. For this purpose both elements are used to study the warpage of a flat unidirectional composite part virtually processed on an aluminum tool (Fig. 7).

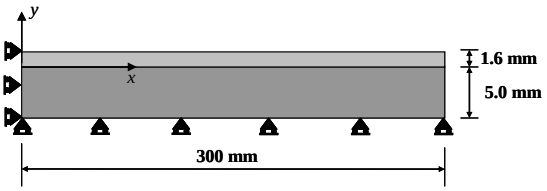

Fig. 7. Schematic of the geometry and boundary conditions used to model the warpage of a flat composite part processed on an aluminum tool (half the length is modelled due to symmetry)

The part is considered to be made of 8 unidirectional layers of T800H/3900-2 CFRP material and subjected to the cure cycle shown in Fig. 8. The material properties are listed in Table 1.

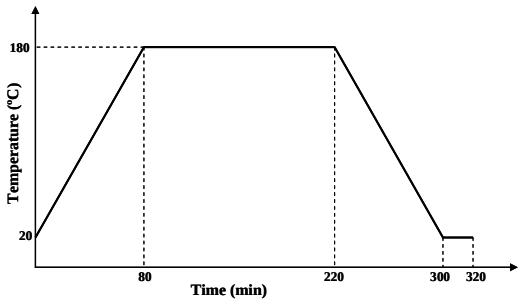

Fig. 8. Typical one-hold temperature cure cycle

This problem was first analysed with the standard 20-noded built-in element in ABAQUS

resulting in a predicted maximum warpage of 35.29 mm using 16 elements in the thickness direction. This is considered to be the converged solution used as benchmark for studying the convergence rates of the *h*- and *p*-elements.

The predicted warpage as a function of the number of d.o.f's in both the *h*- and *p*-element methods is shown in Fig. 9. Note that in all these analyses the part and the tool are assumed to be fully bonded.

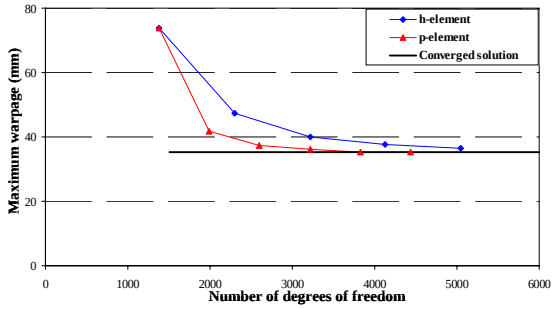

Fig. 9. Comparison of the convergence rates of the *h*- and *p*-element methods

As shown in the figure, the *p*-element converges faster than the *h*-element.

The variation of run time with the number of d.o.f's in both methods is shown in Fig. 10.

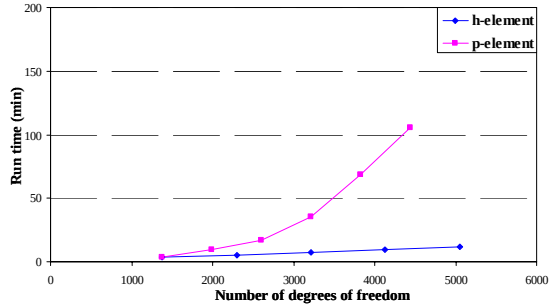

Fig. 10. Comparison of the computational run times of the *h*- and *p*-element methods

In the *p*-element method, the run time is seen to increase exponentially with the number of d.o.f's. Though the implementation of the *p*-element method is more somewhat simpler, it is not as efficient as the *h*-element method in terms of run time. Selection of the number of terms or the number of element layers and suggested techniques to reduce the run time of the *p*-element method will be discussed next.

4 Selection of Number of Terms or Number of Element Layers

In the closed-form solution developed by the authors [2], it is shown that the through-thickness distribution of the axial displacement, *u*, is an exponential function which depends on the material and geometrical properties of the composite part:

$$u \approx e^{\beta \bar{y}}$$
$$\beta = \frac{\pi t}{2l}\sqrt{\left(\frac{E_{11}}{G_{13}}\right)} \qquad (12)$$

where $\bar{y}$ is a non-dimensional thickness coordinate that varies from 0 to 1.0. Taylor series expansion of *u* results in:

$$u \approx 1+\frac{\beta\bar{y}}{1!}+\frac{(\beta\bar{y})^2}{2!}+\frac{(\beta\bar{y})^3}{3!}+\cdots \approx 1+\beta\bar{y}+C_0\bar{y}^2+C_1\bar{y}^3+\cdots \qquad (13)$$

The additional number of terms, *n* (or number of element layers, *n*/2) required for a particular problem is based on the relative contributions of the higher order terms. The basic 24-noded element has a 2nd order shape function or one element in the thickness direction. The ratio of the last two terms in the series, (C_{n+1}/C_n), are compared with a pre-specified threshold limit. For a given value of *n* if the above ratio falls below the threshold limit, then the contribution of additional terms to the accuracy of the predictions is deemed to be insignificant and the series is truncated beyond the n^{th} term. For the composite part considered in this study, the various ratios (C_{n+1}/C_n) computed during the initial stages of curing (representing a severe case when the displacement gradient through the thickness is highly non-linear), are shown in Fig. 11.

In this study, threshold values of 1.0 and 1.5 are selected for the *h*- and *p*-element methods, respectively

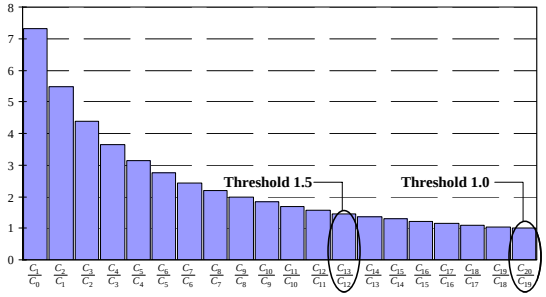

Fig. 11. The ratios of the last two coefficients of the Taylor series expansion of the through-thickness axial displacements used to determine the required number of d.o.f's in *h*- and *p*-element methods

4.1 Reducing the Run Time in the *p*-Element Method

The run time of the *p*-element method may be reduced by: (1) employing an efficient spatial integration technique, and/or (2) dynamically changing the number of terms in the series [10-11]. The second option will be pursued here.

As noted in the previous section, higher order terms may be necessary only at the initial stages of the curing process when the gradient of the through-thickness stress distribution is appreciable. For the above example, the number of higher order terms necessary during the cure cycle to achieve convergence based on a threshold value of 1.5 is shown in Fig. 12.

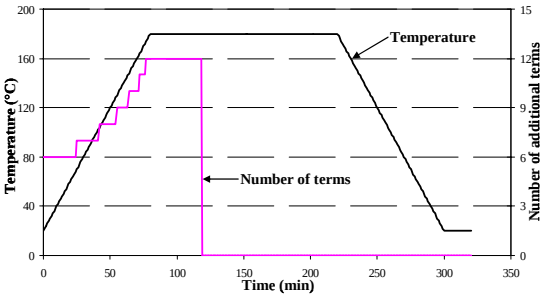

Fig. 12. Number of higher order terms required during the cure cycle to achieve convergence with *p*-elements

As shown in the figure, higher order terms are only necessary during the initial stages of the cure cycle.

4.2 Implementation in ABAQUS

To enable adaptive change in the number of terms, the d.o.f's at the mid-surface nodes need to be altered dynamically. At present, the finite element code ABAQUS does not allow such manipulation of the d.o.f's during the computational run. For user elements, the number of nodes and d.o.f's at each node need to be predefined and remain fixed. A work-around to achieve reasonable run time efficiencies with the existing capabilities of ABAQUS is to run the analysis in two steps (see Fig. 13), where in the first step the maximum number of higher order terms are used followed by a second step where only the basic 24-noded element without any additional hierarchical terms is employed.

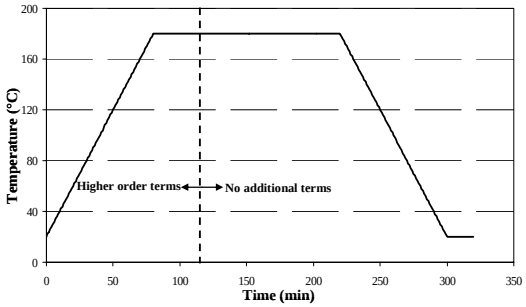

Fig. 13. Cure cycle divided into two regimes to achieve a more efficient *p*-element solution

In order to implement the above, the d.o.f's are activated by dynamically changing the boundary conditions during the run. In this case, the mid surface nodes of the element are assigned the highest number of terms necessary for that particular problem. The latter is a user defined input and is read inside the element. The element calculates only the required components of the load vector and stiffness matrix for the active d.o.f's at that time step. The remaining components of the load vector and the stiffness matrix are set to zero. In the input file, the unnecessary d.o.f's are set to zero using prescribed boundary conditions.

Fig. 14 shows a comparison of the run times using the *h*-element and the *p*-element both with and without adaptivity. As shown in the figure, the run time is substantially reduced (by about 50%) by changing the number of terms in two steps. If the number of steps are increased then the run time can be further decreased. Regardless, the run time of the *p*-element method will still be greater than the *h*-element method. To reduce the run time further, more efficient spatial integration schemes need to be investigated [10-11].

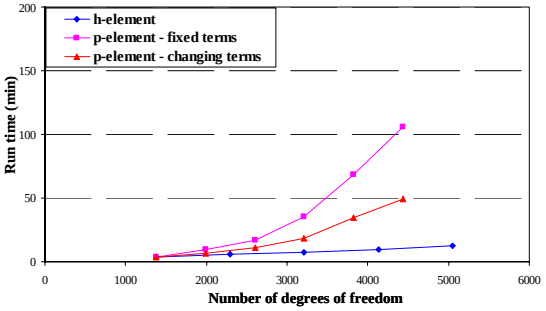

Fig. 14. Comparison of run times between *h*- and *p*-elements

Based on above the example problem, it is apparent that the *h*-element method has many advantages over the *p*-element method such as run time efficiency and the ability to model non-smooth displacement variations through the thickness. Hence, in the following section, the *h*-element element method will be used in concert with the contact surface option in ABAQUS to predict the results of the warpage experiments conducted by Twigg [12].

5 Warpage Predictions

In this section, the experimentally measured warpage of flat unidirectional composite parts of three different lengths (300 mm, 600 mm and 1200 mm) and three different thicknesses (4, 8 and 16 plies) are compared with predictions using the *h*-element method. The tool-part interface condition is simulated using the built-in sliding contact surface in ABAQUS [6].

It was shown in the experiments [13, 14] that a sliding interface condition exists at the early stages of the cure when the resin has a very low modulus. During the temperature hold the part sticks to the tool and during the subsequent cool down it debonds from the tool and slides over it again. Our focus is the sliding interface condition during the heat-up portion of the cure cycle since stresses that develop at the later stages of the cure cycle do not contribute to the unbalanced moment development that lead to part warpage. The basic Coulomb friction model available in ABAQUS with a maximum shear stress limit is used to model the sliding interface condition (Fig. 15)

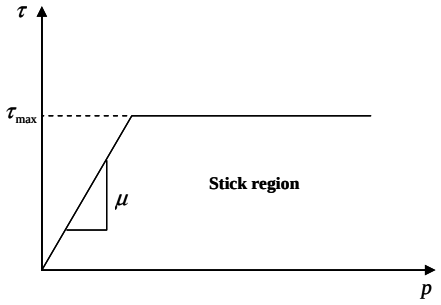

Fig. 15. ABAQUS basic Coulomb friction model with a maximum shear stress limit

Fig. 16 shows a comparison between the predicted and measured warpages. A reasonable agreement is obtained for most cases.

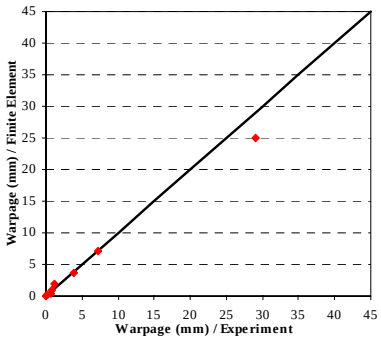

Fig. 16. Comparison of warpage predictions with experimental results

6 Summary and Conclusions

During the processing of thermoset-based composite structures, the thermal strain mismatch between the part and the tool induces a stress gradient through the thickness of the part. In order to predict the residual deformation of the composite part accurately, it is crucial to capture the rather steep and highly non-linear stress gradient that occurs at the initial stages of cure. The magnitude and shape of this stress distribution depends on the material and geometrical properties of the part. Using standard solid elements for process modeling requires a certain element resolution through the thickness in order to achieve accurate solutions. The actual number of elements needed for through-thickness discretization varies from problem to problem. Determining the number of elements by trial-and-error is a tedious and time consuming task as it involves successive mesh refinements.

In this study, two adaptive finite element techniques were developed such that only one

element can be used in the thickness direction to study different problems thus greatly reducing the set-up time. The two developed finite elements were based on the adaptive *p*- and *h*-element method available in the literature. Both methods use a 24-noded subparametric element as the base. By adding the required additional d.o.f's to the mid-surface nodes, the number of terms in the *p*-method and the number of elements in the *h*-method can be increased without changing the original mesh. A methodology was developed to select the number of elements or the number of terms automatically based on the material and geometrical properties.

It was shown that the developed *h*-element is more efficient in terms of run time compared to the *p*-element. The developed *h*-element was used together with the contact surface option in ABAQUS to predict the experimentally observed warpage of flat composite parts.

7 Acknowledgements

The authors would like to thank the Natural Sciences and Engineering Research Council of Canada (NSERC) for their financial support. We would also like to acknowledge many fruitful discussions with colleagues at UBC Composites Group.

References

[1] Johnston, A.A., Vaziri, R., Poursartip, A., "A Plane Strain Model for Process-Induced Deformation of Laminated Composite Structures", J. Composite Materials, **35**(16), pp. 1435-1469, 2001.

[2] Arafath A.R.A., Vaziri R., Poursartip A., "Closed-Form Solution for Process-Induced Stresses and Deformation of a Composite Part Cured on a Solid Tool: Part I – Flat Part ", To be submitted to Composites Part A.

[3] Dhondt, G.D., "The Right Solid Element: a Challenge to Industry", Proceeding of the Fifth World Congress on Computational Mechanics (WCCM V), Vienna, Austria, 2002.

[4] Zienkiewicz, O.C., Gago, J.P., Kelly, D.W., "The Hierarchical Concept in Finite Element Analysis", Comput & Struct., **16**(1-4), pp. 53-65, 1983.

[5] Babuska, I., and Suri, M., "The p and hp Version of the Finite Element Method, Basic Principles and Properties", SIAM Review, **36**(4), pp. 578-632, 1994.

[6] Arafath A.R.A., Vaziri R., Poursartip A., "Higher Order Elements in the Process Modelling of Shell-Like Composite Structures", To be submitted to International Journal for Numerical Methods in Engineering.

[7] ABAQUS, Version 6.4, ABAQUS Inc., 2003.

[8] Arafath A.R.A., Vaziri R., Poursartip A., "Modular Approach to Process Modelling of Composite Structures", To be submitted to Journal of Composite Materials.

[9] Robbins, D.H., and Reddy, J.N., "Modelling of Thick Composites using a Layerwise Laminate Theory", International Journal for Numerical Methods in Engineering, **36**(2), pp. 655-677, 1993.

[10] Hinnant, H.E., "A Fast Method of Numerical Quadrature for *p*-Version Finite Element Matrices", International Journal for Numerical Methods in Engineering, **37**(6) , pp. 3723-3750, 1994.

[11] Nubel, V., Duster, A. and Rank, E., "Adaptive Vector Integration as an Efficient Quadrature Scheme for *p*-Version Finite Element Matrices", ECCM-2001: European Conference on Computational Mechanics, Cracow, Poland, 2001.

[12] Twigg, G., Poursartip, A., Fernlund, G., "Tool-Part Interaction in Composites Processing. Part I: Experimental Investigation and Analytical Model", Composites: Part A, **35** (1), pp. 121-133, 2004.

[13] Twigg, G., Poursartip, A., Fernlund, G., "An experimental method for quantifying tool-part shear interaction during composites processing", Composites Science and Technology, **63**(13), pp. 1985-2002, 2003.

[14] Ersoy, N., Potter, K., Wisnom, M.R., "An Experimental Method to Study the Frictional Processes during Composite Manufacturing", Composites Part A, **36**(11), pp. 1536-1544, 2005.